Supporting Information

Rosenzweig et al. 10.1073/pnas.1512783112

SI Materials and Methods

Translational Diffusion. Translational diffusion coefficients were measured by recording a series of 1D ^{13}C-edited spectra, 25 °C, using a pulse scheme that is similar to an ^{15}N-edited experiment published previously with ^{15}N and ^{13}C pulses interchanged (35). A diffusion delay of 200 ms was used in conjunction with encode/decode gradient strengths ranging from 5 to 54 G/cm. The resulting ^{1}H signal was integrated over the methyl ^{1}H frequency range to obtain intensities as a function of encoding/decoding gradient strength.

T_1, T_2, and Heteronuclear ^{1}H–^{15}N NOE Measurements. Measurements of backbone ^{15}N R_1 and R_2 relaxation rates and steady-state heteronuclear ^{1}H–^{15}N NOEs (HNOEs) were carried out on a 1 mM uniformly ^{15}N-enriched NTD sample at 25 °C, 14.1 T, using TROSY-based pulse schemes (2). The ^{15}N R_1 data were acquired using relaxation delays ranging from 10 to 1,150 ms while ^{15}N $R_{1\rho}$ rates were quantified using relaxation delays from 2 to 80 ms. R_2 values were calculated from R_1 and $R_{1\rho}$ rates according to the equation $R_{1\rho} = R_1\cos^2\theta + R_2\sin^2\theta$, where $\theta = \arctan(\omega_{SL}/\Delta\omega)$, $\Delta\omega$ is the resonance offset from the spin-lock carrier, and ω_{SL} is the spin-lock field strength (1.84 kHz). Values of relaxation rates were obtained by nonlinear least-squares fitting of the experimental data to a monoexponential decay function, $A\exp(-R_iT)$, $R_i = \{R_1, R_{1\rho}\}$. Heteronuclear NOE values were obtained by recording spectra in the presence (7-s relaxation delay) and absence (13-s relaxation delay) of a ^{1}H saturation period of 6 s. Values of R_1, R_2, and NOE were fitted using the model-free approach with ModelFree4 software (55) assuming isotropic overall motion, to extract a single correlation time (τ_C) and residue-specific values of order parameters squared (S^2) and effective internal correlation times (τ_e).

Measurement of Methyl ^{1}H R_{2s} Rates. Residue-specific relaxation rates of slowly relaxing methyl ^{1}H single-quantum transitions were measured using the pulse scheme of Tugarinov and Kay (36). A set of 2D ^{13}C, ^{1}H datasets were recorded where a relaxation delay, T, was varied from 1–20 ms for segmentally labeled hexameric ClpB (NTD-[^{2}H, ^{13}CH$_3$-ILVM], ClpB$^{\Delta N}$-[^{2}H, ^{12}C]) and from 1 to 100 ms for the monomeric NTD. R_{2s} rates were obtained from exponential fits of peak intensity, I, as a function of relaxation delay, using the relation $I = I_o\exp(-R_{2s}T)$.

Measurement of $S^2_{axis}\tau_c$ Values. Methyl group $S^2_{axis}\tau_c$ values were measured on samples of segmentally labeled hexameric ClpB (NTD-[^{2}H, ^{13}CH$_3$-ILVM], ClpB$^{\Delta N}$-[^{2}H, ^{12}C]) and on monomeric [^{2}H, ^{13}CH$_3$-ILVM]-labeled NTD. Data analysis was as described in ref. 37 using an approach that quantifies the time dependencies of sums (I_{allow}) and differences (I_{forb}) of magnetization derived from methyl ^{1}H single- and triple-quantum transitions, respectively. For hexameric ClpB, I_{allow} and I_{forb} were measured at 55 °C with relaxation time (T) values of 1, 2, 3, 4, 5, 6, 7, 8, 9, 10, 12, 14, and 16 ms, whereas for the monomeric NTD values were obtained at 25 °C using delays of T = 2, 4, 7, 10, 15, 20, 25, 30, 35, 40, 45, and 50 ms. The profiles I_{forb}/I_{allow} were fitted to the following:

$$\left|\frac{I_{forb}}{I_{allow}}\right| = \frac{0.75\eta\,\tanh\left(\sqrt{\eta^2+\delta^2}T\right)}{\sqrt{\eta^2+\delta^2} - \delta\tanh\left(\sqrt{\eta^2+\delta^2}T\right)}, \qquad [S1]$$

where

$$\eta \cong \frac{9}{10}\left(\frac{\mu_0}{4\pi}\right)^2\left[P_2\left(\cos\left(\theta_{axis,\,HH}\right)\right)\right]^2\frac{S^2_{axis}\gamma_H^4\hbar^2\tau_c}{r_{HH}^6}. \qquad [S2]$$

In Eq. **S1**, η is as given in Eq. **S2**, where $P_2(x) = (3x^2 - 1)/2$, $\theta_{axis,HH}$ is the angle (90°) between the methyl threefold axis and the vector that connects a pair of methyl ^{1}H nuclei, τ_C is the assumed isotropic tumbling time of the protein, S^2_{axis} is the square of an order parameter quantifying the amplitude of motion of the methyl threefold symmetry axis, $\hbar$ is Planck's constant divided by 2π, γ_H is the gyromagnetic ratio of a proton spin, and r_{HH} is the distance between pairs of methyl protons (1.813 Å). The parameter δ in Eq. **S1** takes into account the ^{1}H density around the methyl group in question. Values of $S^2_{axis}\tau_C$ measured for the NTD were used to obtain S^2_{axis} values on a per-residue basis assuming a value for τ_C from ^{15}N spin relaxation experiments discussed above. The resultant order parameters were subsequently extrapolated to 55 °C by assuming temperature-dependent changes in S^2_{axis} values as described in ref. 56. These extrapolated order parameters were then used to obtain per-residue values of τ_C for methyl probes attached to the NTD of segmentally labeled ClpB for which $S^2_{axis}\tau_c$ values had been measured. To compare correlation times for the attached NTD and the "rigid" regions of the assumed isotropically tumbling hexameric ClpB complex a value of τ_C = 180 ns, 55 °C, based on the estimated value of τ_C = 120 ns for the *Thermoplasma acidophilum* $\alpha_7\alpha_7$ complex, 50 °C (31), was assumed by taking into account the viscosity dependence of D_2O as a function of temperature (57) as well as the molecular-weight differences between the two particles.

NMR Thermal Melt. Two-dimensional ^{1}H–^{13}C HMQC spectra were collected on a 0.4 mM sample of the Pin1 WW domain, alone and in the presence of 1 mM ClpB NTD, between the temperatures of 15 and 80 °C at intervals of 5 °C. The positions of many peaks shift considerably over the temperature range and can be used to monitor the unfolding of the protein (58), as it is known that Pin1 WW folds via a two-state mechanism (38). A thermal denaturation midpoint temperature, T_m, was determined by fitting changes in chemical shifts on a per-residue basis according to the following equation:

$$\delta = \frac{(b_F + m_F T) + b_U\cdot\exp\left\{\dfrac{-\left(\Delta H\left(1-\dfrac{T}{T_m}\right) + \Delta C_p\left(T - T_m - T\cdot\ln\left(\dfrac{T}{T_m}\right)\right)\right)}{RT}\right\}}{1+\exp\left\{\dfrac{-\left(\Delta H\left(1-\dfrac{T}{T_m}\right) + \Delta C_p\left(T - T_m - T\cdot\ln\left(\dfrac{T}{T_m}\right)\right)\right)}{RT}\right\}}. \qquad [S3]$$

In Eq. **S3**, the chemical shift of a methyl probe in the folded state changes linearly with temperature, T, as $b_F + m_F{}^*T$, whereas the corresponding shift in the unfolded state is temperature independent, b_U; ΔH is enthalpy change from unfolding at T_m; and ΔC_p is the change in heat capacity upon unfolding.

Differential Scanning Calorimetry. Differential scanning calorimetry (DSC) experiments were carried out with a VP-DSC calorimeter from MicroCal at a scan rate of 1.0 K/min. DSC data were analyzed with a two-state unfolding model (59), using theoretical heat capacity baselines for the unfolded state (60) and optimizing a linear heat capacity baseline for the folded state. The fits had five adjustable parameters: the denaturation midpoint, the enthalpy of denaturation at the midpoint, two parameters to describe the linear folded-state baseline, and a vertical offset correction for the

unfolded baseline (61). The analyses were done in triplicate and yielded a denaturation temperature midpoint of 105.4 ± 0.1 °C and ΔH_{ND} = 12.92 ± 0.03 kcal·mol^{-1}.

ClpB ATPase Activity Determination. The ATPase activities of WT or mutant ClpB (10 μM) were measured spectrophotometrically (62) with an ATP-regeneration system that contained 2.5 mM phosphoenolpyruvate, 0.2 mM NADH, 50 μg/mL pyruvate kinase, 50 μg/mL lactate dehydrogenase, and 3 mM ATP at 55 °C (63). When indicated, α-casein (0.1 mg/mL), p13 (50 μM), peptide B1 (50 μM), or an ATP hydrolysis inactive T199A mutant of DnaK (25 μM), was added to the reaction. The changes in absorbance at 340 nm were monitored in a V-650 spectrophotometer. All ATPase assays were performed in triplicate.

Degradation Reactions. All degradation reactions were carried out using 1 μM BAP variants, 1.5 μM ClpP, and 2 μM α-casein supplemented by an ATP regenerating system (63). α-Casein degradation was followed by gel electrophoresis and Coomassie blue staining. The amounts of remaining substrate at the indicated time points (0, 5, 10, 15, 30, 60, and 120 s) were quantified using ImageJ software.

Disaggregation Reactions. Recombinant firefly luciferase (0.2 μM) was incubated for 30 min at 30 °C in denaturation buffer (25 mM Hepes-KOH, pH 7.5, 50 mM KCl, 10 mM $MgCl_2$, 1 mM DTT, 6 M urea). To form irreversible aggregates, denatured luciferase was diluted 125-fold into renaturation buffer at 4 °C (25 mM Hepes, pH 7.5, 50 mM KCl, 10 mM $MgCl_2$, 1 mM DTT, 0.1 mg/mL BSA, 1 mM ATP, 20 mM creatine phosphate, 6 μg of creatine kinase). The refolding reaction was initiated through the addition of 5 μM WT ClpB or mutants of ClpB, 3 μM DnaK, 0.8 μM DnaJ, and 0.4 μM GrpE to 2 nM luciferase aggregates. Luminescence was measured following 2 h of disaggregation and subsequent addition of 50 μM luciferase reagent (Promega) to 2 μL of the refolding reaction.

α-Glucosidase from *Bacillus stearothermophilus* (Sigma) (0.1 μM) was denatured for 10 min at 75 °C in reaction buffer (25 mM Hepes-KOH, pH 7.5, 50 mM KCl, 10 mM $MgCl_2$). Chaperones were then added (3.5 μM WT ClpB or mutants of ClpB, 3.0 μM DnaK, 0.8 μM DnaJ, 0.2 μM GrpE) before refolding at 37 °C. Following 2 h of disaggregation, the recovered α-glucosidase activity was measured as described previously (64).

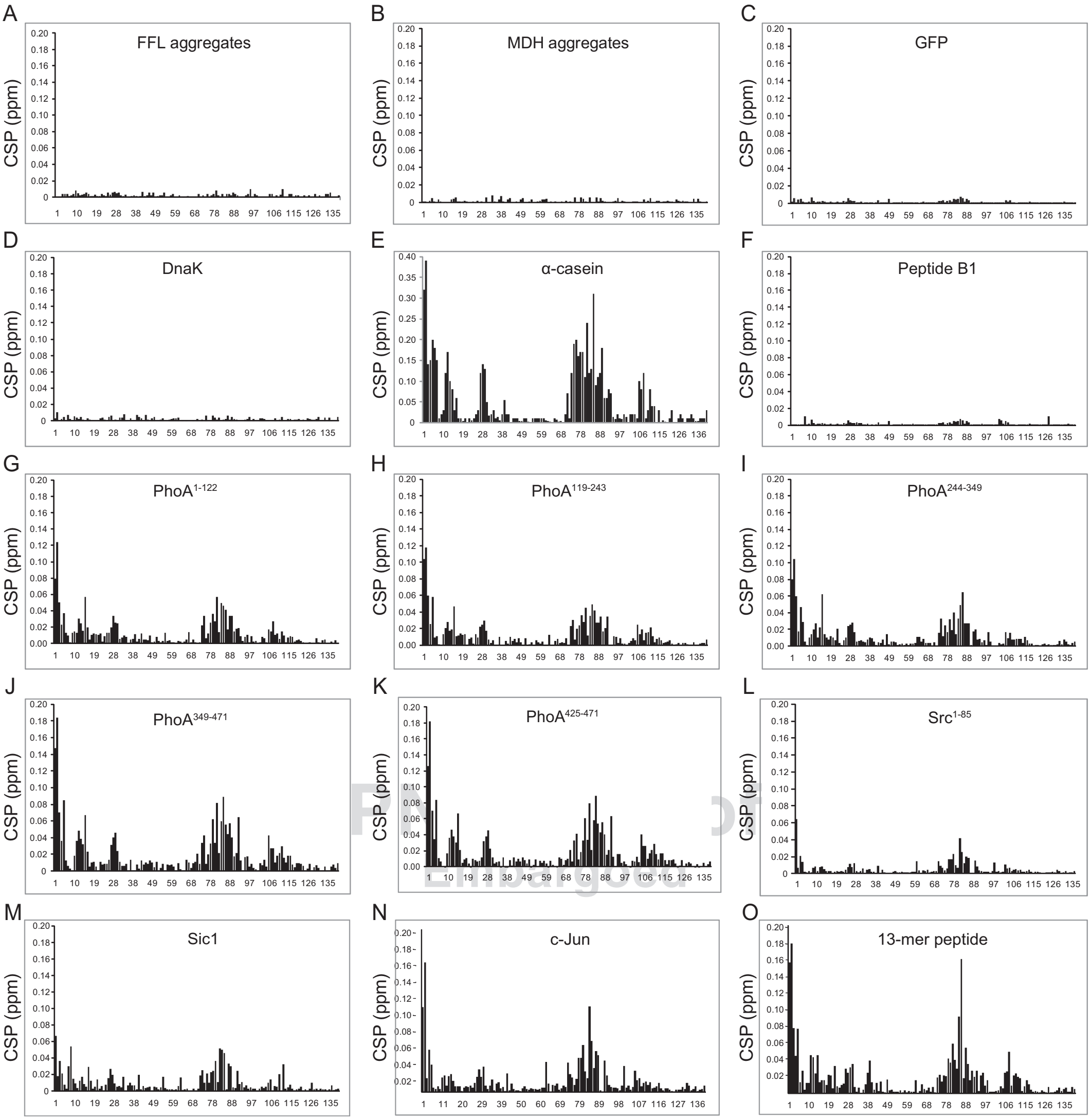

Fig. S1. Substrate interactions with NTD. Chemical shift perturbations (CSPs), plotted by residue number, of [^{1}H, ^{15}N]-labeled monomeric NTD upon binding to 3 molar equivalents of (*A*) chemically denatured firefly luciferase (FFL) aggregates, (*B*) heat-induced malate dehydrogenase (MDH) aggregates, (*C*) green fluorescent protein (GFP), (*D*) DnaK, (*E*) α-casein, (*F*) peptide B1, (*G–K*) reduced alkaline phosphatase (PhoA) fragments, (*L*) Src residues 1–85, (*M*) Sic1, (*N*) c-Jun, and (*O*) p13 (KLDSLIVFLREEA). CSPs were defined by the relation, $\mathrm{CSP} = \sqrt{(\Delta\delta_{\mathrm{H}})^2 + (\Delta\delta_{\mathrm{N}}/5)^2}$, where $\Delta\delta_{\mathrm{H}}$ and $\Delta\delta_{\mathrm{N}}$ are proton and nitrogen chemical shift changes between apo and bound forms of the protein.

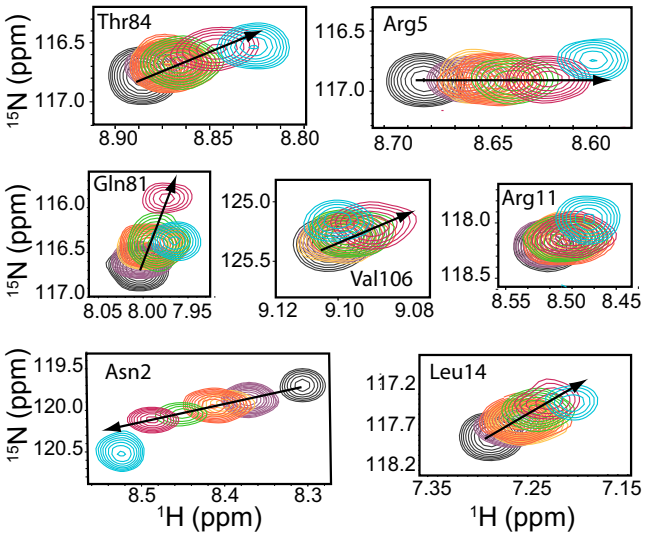

Fig. S2. ClpB NTD rapidly samples different binding sites from client proteins. Overlay of ^{1}H–^{15}N HSQC spectra of ClpB NTD alone (in black) and in the presence of twofold excess of PhoA$^{1\text{-}121}$ (red), PhoA$^{119\text{-}243}$ (yellow), PhoA$^{244\text{-}349}$ (purple), PhoA$^{349\text{-}471}$ (green), α-casein (maroon), or p13 (cyan) for selected NTD residues. Trajectories of the shifts are linear for all substrates (indicated by an arrow), with the exception of p13. The NTD–substrate complex is highly dynamic with the chemical shifts representing an average over a range of different environments. Shifts for p13 (cyan) do not lie on the same line as the rest of the substrates, as the peptide contains a single optimal NTD binding site and forms a stable (not averaged) complex.

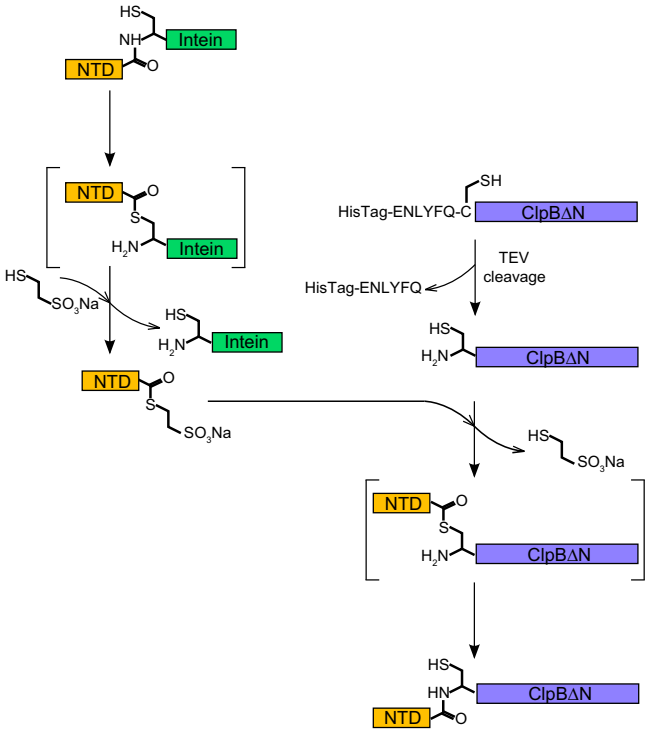

Fig. S3. Segmental labeling scheme for hexameric ClpB. To produce a hexameric ClpB protein, segmentally labeled at the NTD, NTD-intein fusion, and NBD1-CCD-NBD2 (ClpB$^{\Delta N}$) ClpB regions were grown separately in M9 D_2O minimal media supplemented with $^{14}NH_4Cl$ and [^{2}H,^{12}C]-glucose as the sole nitrogen and carbon sources, respectively. Methyl labeling precursors were added to the growth media of the NTD [Ile-δ1-[$^{13}CH_3$] and Val/Leu-[$^{13}CH_3$, $^{12}CD_3$] (28)], but not to the ClpB$^{\Delta N}$ prep so that ClpB$^{\Delta N}$ will be "NMR invisible." Both NTD-intein and ClpB$^{\Delta N}$ were purified as described in *Materials and Methods*. (*Left Down*) Cleavage of NTD from the intein fusion occurs via the following steps: (*i*) N → S acyl shift of cystein at the intein N terminus results in the formation of a reactive thioester. (*ii*) Thiol-mediated cleavage: a nucleophilic attack on the thioester by a small thiol compound (MESNA) cleaves the precursor protein and generates a new thioester at the C terminus of the target protein. (*Right Down*) The ClpB$^{\Delta N}$ N-terminal tag is cleaved via TEV protease exposing an N-terminal cystein. The subsequent ligation reaction between ClpB$^{\Delta N}$ and ClpB NTD involves attack of the activated thioester in NTD by the α-Cys residue of ClpB$^{\Delta N}$. Next, spontaneous rearrangement of the thioester (via S → N acyl shift) results in the formation of a peptide bond between the two domains. The ligation procedure introduces a single cystein substitution at the ligation junction.

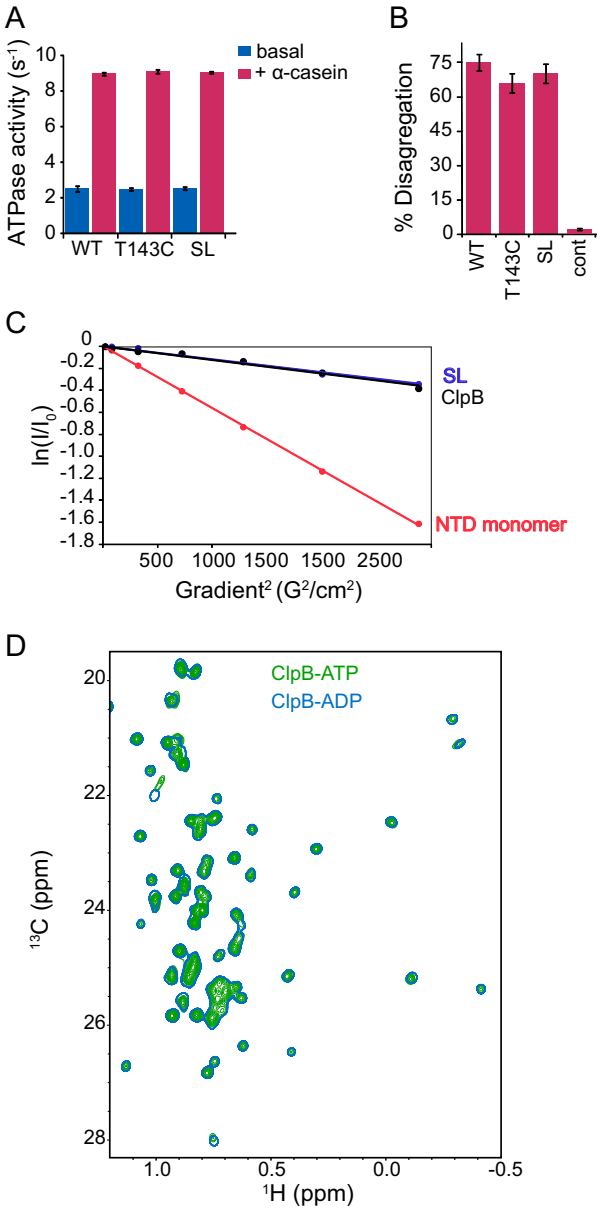

Fig. S4. Characterization of segmentally labeled hexameric ClpB. (*A*) ATPase activities of $ClpB^{WT}$, $ClpB^{T143C}$, and segmentally labeled (SL) ClpB measured in the absence (blue) or the presence (maroon) of 0.1 mg/mL α-casein. ATPase activities are expressed as turnover per monomer ClpB. (*B*) Disaggregation activity of the same ClpB variants in the presence of the DnaK, DnaJ, GrpE chaperone system. Amounts of reactivated firefly luciferase after 120-min incubation are expressed as a percentage of the activities before chemical inactivation. Average values from three separate experiments are shown along with SDs. The entry "cont" refers to control experiments performed in the absence of luciferase. Neither the T143C mutation nor the segmental labeling ligation procedure had any measurable effect on the ATPase (*A*) and DnaK-dependent disaggregation activities (*B*). (*C*) Translational diffusion coefficients were measured for a methyl-labeled ClpB sample, a segmentally methyl-labeled ClpB sample, and a monomeric NTD (16 kDa) using a variant of the SLED experiment that contains ^{13}C editing (1). The slope of the ln(intensity) vs. squared gradient profile in each of the curves is proportional to the diffusion constant and inversely proportional to the cube root of the molecular weight, assuming that each of the diffusing particles is spherical. Diffusion coefficients for the two ClpB samples were identical to within error ($1.28 \pm 1.1 \times 10^{-7}$ and $1.23 \pm 0.6 \times 10^{-7}$ cm^2/s, respectively), indicating that the segmentally labeled sample also forms hexamers. The 16-kDa NTD diffused much more rapidly ($5.7 \pm 0.1 \times 10^{-7}$ cm^2/s), as expected. (*D*) Overlay of selected regions of ^{1}H–^{13}C HMQC correlation maps of segmentally labeled hexameric ATP-bound (green) and ADP-bound (blue) ClpB. No significant changes in spectra were observed between ATP- and ADP-bound states, with the exception of residues located in the linker connecting the NTD to NBD1.

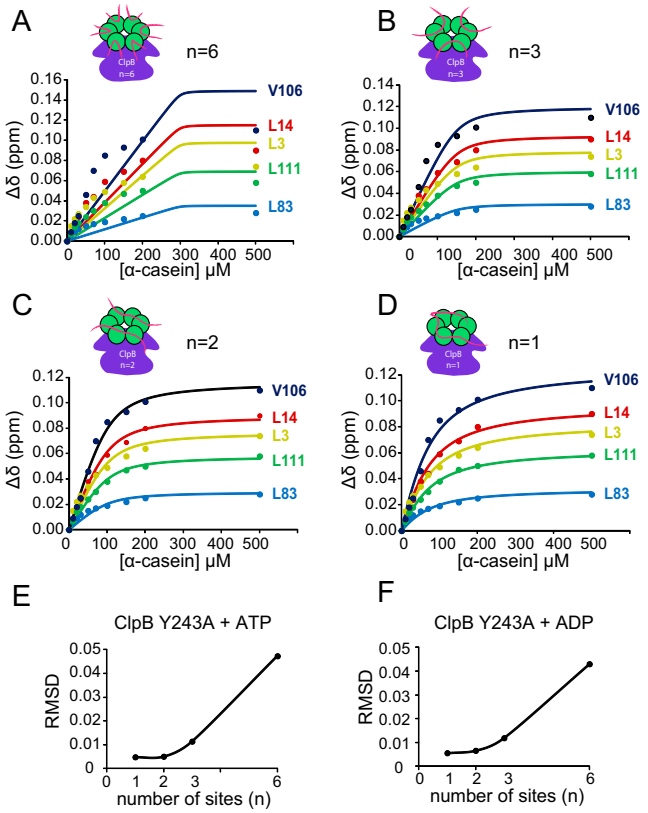

Fig. S5. Multiple NTDs simultaneously bind to a client protein. Titration curves reporting changes in ^{1}H chemical shifts ($\Delta\delta$, in parts per million) of methyl probes of ClpB^{Y243A} as a function of α-casein concentration. The isotherms are fit to models (solid lines) assuming (*A*) each of the six NTDs in the ClpB hexamer binds one α-casein molecule, (*B*) two NTDs are required for binding to a single α-casein, (*C*) three NTDs interact with a single α-casein, or (*D*) all six NTDs bind a single α-casein molecule. A schematic of each binding possibility is shown, with *n* the number of casein molecules required to saturate a ClpB hexamer. Dissociation constants (K_D) were obtained by fitting experimental data to the appropriate equation as described in *Materials and Methods*. (*E* and *F*) RMSD plots showing the deviation of the calculated and experimental chemical shifts (in parts per million) based on fits of titration data for ATP-ClpB^{Y243A} (*E*) and ADP-ClpB^{Y243A} (*F*). Notably, good fits were obtained for $n = 1$ and $n = 2$, where six or three NTDs, respectively, are assumed to bind to a single α-casein.

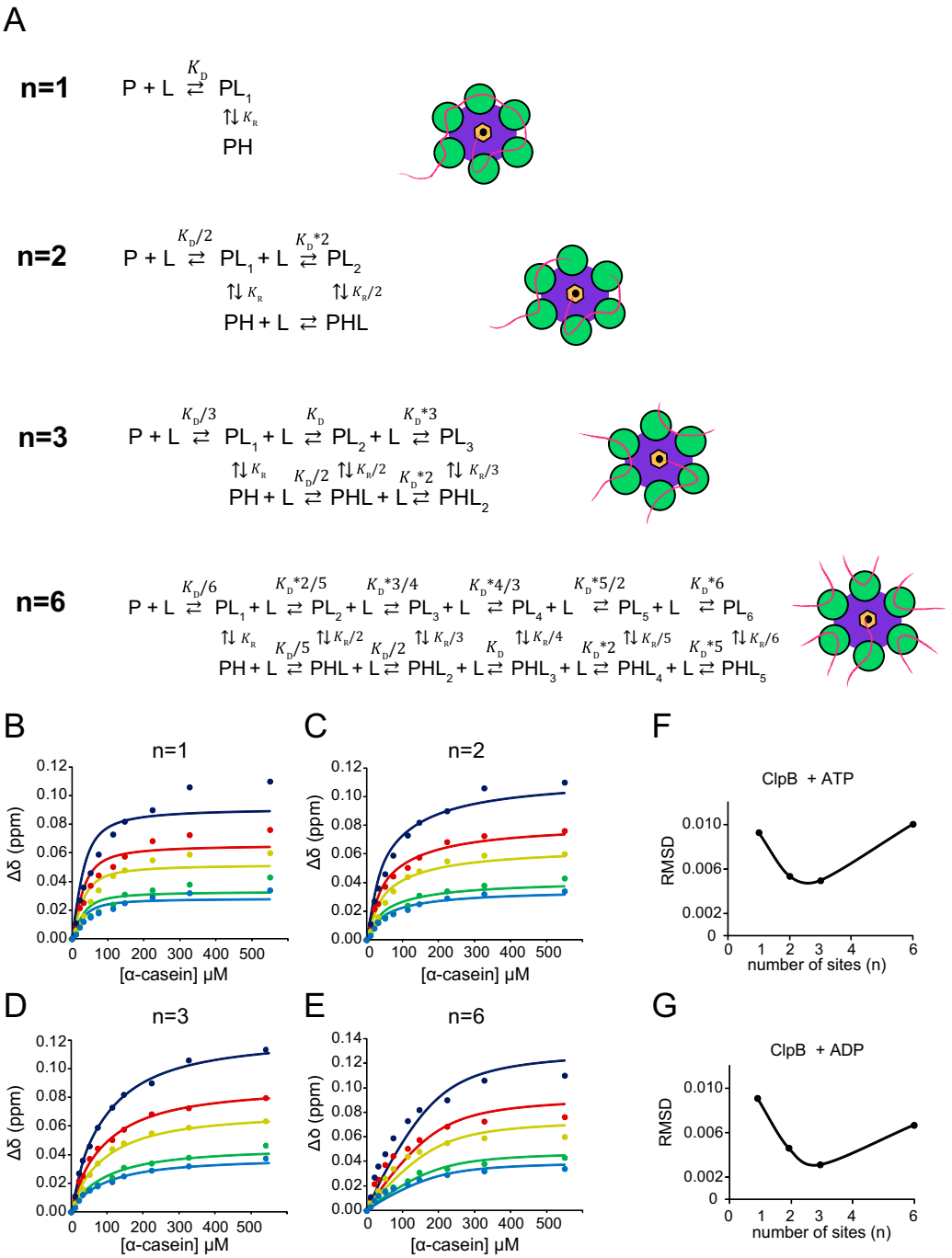

Fig. S6. Interaction of WT hexameric ATP- and ADP-bound ClpB with α-casein. (*A*) Binding schemes representing different scenarios for the interaction of α-casein with hexameric ClpB, with *n* the number of ligand molecules (α-casein) bound to one ClpB hexamer. Each scheme assumes that a molecule of α-casein binds to a different number of NTDs, with $n = 1$ denoting one α-casein per six NTDs (i.e., one binding site per ClpB hexamer), $n = 2$ corresponding to two binding sites (each binding site comprises three NTDs), and so forth. This is illustrated schematically where the purple line denotes a ligand, each of the green circles is an NTD, and the tyrosine pore is depicted in yellow. In each of the schemes, P and L are protein (ClpB) and ligand (α-casein), respectively, PL_k corresponds to the case where *k* α-casein molecules are bound to ClpB (one ligand per 6/*n* NTDs corresponding to the *n* NTD binding sites in each of the models above), PHL_{k-1} corresponds to ClpB with *k* bound ligands, 1 that is bound to 6/*n* NTDs and the tyrosine pore site simultaneously, whereas the remaining $k - 1$ ligands are bound exclusively to NTDs. Thus, in the case of $n = 3$, each ligand binding event involves interaction of α-casein with a pair of NTDs so that PL_1 is ClpB bound to one ligand (involving two NTDs) that does not engage the tyrosine pore site and PH denotes the case when the ligand is bound to both NTD and the pore. Note that only a single ligand can engage the tyrosine pore site and that this engagement can occur only after binding to the first ligand binding site in the ClpB ring (i.e., to at least 6/*n* NTDs in each of the models above), although it does not have to. The basis for the fact that binding to NTDs must precede binding to the tyrosine pore site is shown in Fig. 6*E*, where if binding to the NTD is knocked out there is no engagement with the pore and subsequent translocation. Note that each NTD binding event, as depicted by the horizontal traces above ($P + L \ldots PL_n$), is assumed to be independent of all others and to occur with the same microscopic association constant, $1/K_D$. The appropriate multiplicative factors associated with each K_D value can be derived by counting the number of ways that a ligand can bind to each of the states. The ratio K_R is defined as [PL1]/[PH] and the affinity that ligand has for the pore is independent of whether the pore binding event occurs immediately after the first substrate binds NTDs or after subsequent ligand binding events (the multiplicative factors

Legend continued on following page

for each K_R take into account the number of ways that k bound substrates can engage a single pore, for example). The product $K_D \cdot K_R$ can be thought of as the overall equilibrium dissociation constant of a ligand molecule that is engaged both by the NTDs and the tyrosine pore. (*B–E*) Titration curves reporting changes in chemical shifts of methyl probes of ClpB^{WT}-ADP as a function of α-casein concentration fit to models (solid lines) indicated in *A*, assuming (*B*) all six NTDs bind a single α-casein molecule, $n = 1$, (*C*) three NTDs interact with a single α-casein, $n = 2$, (*D*) two NTDs are required for binding a single α-casein, $n = 3$, or (*E*) each of the six NTDs in the ClpB hexamer binds one α-casein molecule, $n = 6$. (*F* and *G*) $\Delta\delta$ RMSD plots showing the deviation of the fitted chemical shifts from the experimental values (in parts per million) for ATP-ClpB^{WT} (*F*) and ADP-ClpB^{WT} (*G*) titrations with α-casein.

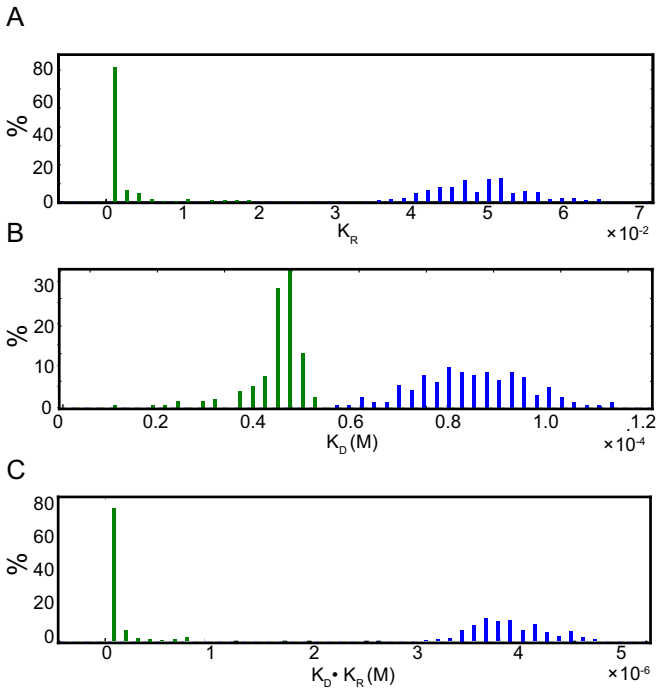

Fig. S7. The affinity of the tyrosine pore for substrate is nucleotide dependent. Histograms showing the distribution of fitted K_R (*A*), K_D (*B*), and $K_D \cdot K_R$ (*C*) values for the binding of α-casein to ATP-ClpB (green) and ADP-ClpB (blue). Distributions were obtained using a bootstrap procedure (51) involving 200 trials.

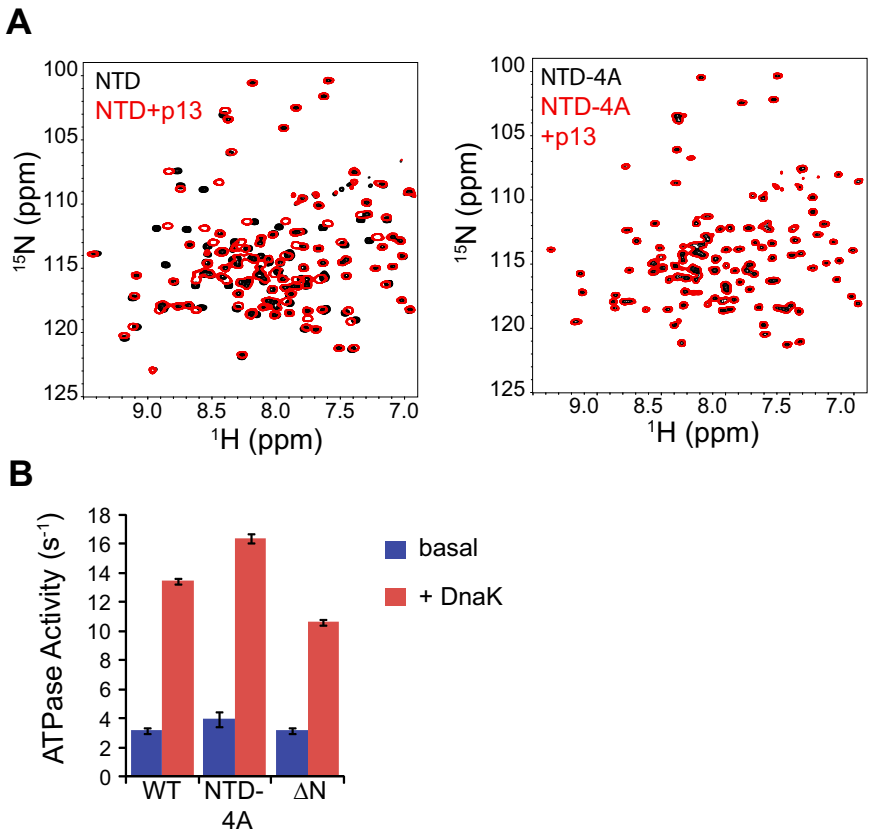

Fig. S8. Hydrophobic residues in the NTD are required for interaction with substrates. (*A*) Superposition of selected regions of ^{1}H–^{15}N HSQC spectra of the uniformly ^{15}N-labeled NTD (*Left*) or NTD-4A (W6A, L14A, L91A, L111A) (*Right*) with (red) or without (black) threefold excess p13. There are no changes to the spectrum of NTD-4A upon addition of p13. (*B*) ATPase activities of ClpB^{WT} (WT), ClpB$^{NTD\text{-}4A}$ (NTD-4A), and ClpB$^{\Delta N}$ (ΔN) measured in the absence (blue) or the presence (maroon) of DnaK. Average values from three separate experiments are shown along with SDs. ClpB$^{NTD\text{-}4A}$ shows WT level ATPase activity and fourfold activation by the DnaK chaperone.

Table S1. Binding affinities for a range of NTD substrates

Protein	Molecular weight, kDa	PI	K_D, μM	Protein type
α-Casein	~23	4.7	107 ± 23	IDP
PhoA$^{1\text{-}121}$ (P1)	12.8	9.0	281 ± 73	Unfolded
PhoA$^{119\text{-}243}$ (P2)	12.3	5.3	268 ± 62	Unfolded
PhoA$^{244\text{-}349}$ (P3)	11.5	6.8	243 ± 42	Unfolded
PhoA$^{349\text{-}471}$ (P4)	12.9	5.0	181 ± 56	Unfolded
PhoA$^{1\text{-}62}$	6.4	8.3	311 ± 57	Unfolded
PhoA$^{425\text{-}471}$	4.9	4.9	255 ± 35	Unfolded
Sic1	9.6	12.2	342 ± 88	IDP
c-Jun	13.4	5.3	289 ± 58	IDP
Src$^{1\text{-}85}$	8.4	10.2	396 ± 74	IDP
p13	1.3	4.3	320 ± 60	Peptide

Affinities quantified from fits of chemical shift changes in titration spectra of U-[^{1}H,^{15}N] NTD as a function of added substrate. All measurements were at 55 °C. IDP, intrinsically disordered protein.

Table S2. Binding affinities of α-casein or 13-mer peptide to ClpB variants and NTD

ClpB variant	Substrate	Nucleotide	*N**	K_D, μM
$ClpB^{Y243A}$	α-Casein	ATP	6	29 ± 4
$ClpB^{Y243A}$	α-Casein	ADP	6	43 ± 6
$ClpB^{WT}$	α-Casein	ATP	2	46 ± 5 (NTD) (<0.09)† (Y243)
$ClpB^{WT}$	α-Casein	ADP	2	85 ± 12 (NTD) 4 ± 0.4 (Y243)
$ClpB^{Y243A}$	p13	ATP	1	380 ± 80
NTD	α-Casein	—	1	98 ± 23
NTD	p13	—	1	390 ± 50

Affinities derived from fits of chemical shift changes in ^{1}H–^{13}C HMQC spectra of $^{13}CH_3$-ILV–labeled ClpB variants as a function of added substrate. All measurements were performed at 55 °C.

*Number of ClpB NTDs involved in the interaction with a single substrate molecule. *N* is related to *n*, the number of casein or p13 ligands that bind to ClpB (Figs. S5 and S6) according to $6/N = n$.

†Y243 corresponds to binding to the tyrosine pores. Measurement of nanomolar K_D values is very difficult by NMR. An upper value of 90 nM is reported here, which encompasses 85% of the values obtained from a bootstrap analysis of the titration data (Fig. S7).